Int. J. Electrochem. Sci., 15 **(2020)** 9981 – 10006, doi: 10.20964/2020.10.03

International Journal of
ELECTROCHEMICAL
SCIENCE
www.electrochemsci.org

Error Analysis of Model-based State-of-Charge Estimation for Lithium-Ion Batteries at Different Temperatures

Zhong Ren[1,2], *Changqing Du*[1,2 *] , *Huawu Wang*[3] *and Jianbo Shao*[1,2]

[1] Hubei Key Laboratory of Advanced Technology for Automotive Components, Wuhan University of Technology, Wuhan 430070, China;
[2] Hubei Collaborative Innovation Center for Automotive Components Technology, Wuhan University of Technology, Wuhan 430070, China;
[3] Dongfeng Commercial Vehicle Co. Ltd., Wuhan 430070, China.
[*]E-mail: cq_du@whut.edu.cn

Received: 2 June 2020 / *Accepted:* 16 July 2020 / *Published:* 31 August 2020

State-of-charge (SOC) estimation of lithium-ion batteries (LIBs) is one of the core functions of a battery management system (BMS). Until now, numerous approaches have been proposed to achieve high-accuracy SOC estimation, among which the model-based SOC estimation algorithm is the most popular algorithm implementation in an actual BMS. Since SOC estimation accuracy is directly influenced by battery model accuracy, it is essential to quantitatively analyze the relationship between model and SOC estimation accuracy, as well as the error sources of the model error. In this article, first, the model accuracy and SOC estimation accuracy are comprehensively studied based on the first-order resistance-capacitor (RC) model and extended Kalman filter (EKF) algorithm under the constant current discharge (CCD) test and Federal Urban Dynamic Schedule (FUDS) test at different test temperatures (0°C, 10°C, 20°C, 30°C, 40°C, and 50°C). Second, regression and correlation analysis is applied to quantitatively evaluate the relationship between the normalized root-mean-square error (RMSE) of model and SOC estimation error. Third, the impact of the SOC open-circuit-voltage (OCV) curve, Ohmic resistance, impedance, and sensor error on SOC estimation accuracy are systematically studied as well. The results show that there is a one-dimensional linear positive relationship between model and SOC estimation accuracy, and the specific quantitative relationship is given. Among the parameters of the battery model, the accuracy of the SOC-OCV curve has the greatest influence on model and SOC estimation error compared to Ohmic resistance and impedance. In addition, compared to the effect of current sensor error, the voltage sensor error has a more significant impact on model and SOC estimation error.

Keywords: Lithium-Ion Battery; State-of-Charge Estimation; Extended Kalman Filter Algorithm; Error Analysis; Battery Management System

1. INTRODUCTION

Developing electric vehicles (EVs) to replace the conventional petrol-fueled cars is considered a promising way to solve global environmental issues, such as the greenhouse effect, the rise of sea levels, and global warming. Among the numerous types of energy-storage systems, lithium-ion batteries (LIBs) are widely used by EV manufacturers due to their advantages of high energy density, high power density, and long cycle life [1]. To satisfy the high voltage and high energy demands of EVs, LIBs must be connected in series and parallel, which makes the control and usage of batteries more difficult. Furthermore, to protect batteries from damage, prolong their life, and maintain them in a safe operating condition, a battery management system (BMS) is extremely necessary [2]. The fundamental function of a BMS is to supervise the voltage, current, and temperature of each single battery to guarantee a safe operation window, then calculate the indicators of battery state using the data collected and stored, and transfer the information with high-level controllers, such as the vehicle control unit (VCU). Among the state indicators, one of the most important is state of charge (SOC).

SOC is a metric that represents the remaining capacity of a battery and that is considered the fundamental indicator for the other state indicators (e.g., state of health (SOH) and state of power (SOP)). Until now, the existing SOC estimation methods have been divided into three categories [3]: direct calculation, model-based, and data-driven methods. Two widely applied approaches of the direct calculation methods are the look-up table methods and the Coulomb counting method. The look-up table approaches usually use the pre-established mapping relationship calculated from the experimental data between the SOC and several parameters, such as open-circuit voltage (OCV), internal resistance, or impedance to obtain the SOC [4]. However, the main drawback of the look-table approaches is that precise online measurement of these parameters poses a significant challenge. Regarding the Coulomb counting method, despite it being widely considered the easiest way to estimate SOC since it is simply based on the integration of current with respect to time while charging or discharging, it still has some fatal disadvantages, like the initial value, capacity, and accumulative errors caused by current measurement sensors [5]. Other efficient SOC estimation methods, i.e., the data-driven methods, including artificial neural networks (ANNS) [6], support vector machines (SVMs) [7], genetic algorithms (GAs) [8], and fuzzy logic (FL) [9], among others, are also exploited in battery SOC estimation due to their advantages, e.g., strong adaptability, highly non-linear fitting, and no pre-knowledge about the battery. However, these methods are very sensitive to the quality of the training data and training result. Moreover, the application of the data-driven methods in a vehicle-level BMS requires high-demand chips and large memory space, which would result in difficulties in implementation and high cost. In addition to the aforementioned approaches, another effective approach, namely, the model-based method, is widely researched for its relatively high accuracy and simplicity of application.

To apply the model-based SOC estimation algorithm, two important steps are required: selecting an accurate and reliable battery model and exploring a simple and efficient algorithm [10]. The widely used battery model can divided into electrochemical models (EMs), equivalent circuit models (ECMs), and fractional order models (FOMs) [11]. Compared to EMs and FOMs, ECMs are more popular in SOC estimation algorithms for such special advantages as simplified structure, easy identifiability, and clear

physical meanings. Generally speaking, ECMs utilize the electronic components, such as ideal voltage resource, Ohmic resistance, and impedance, to simulate the non-linear characteristic of a battery by which the ECMs can keep a balance between simulation accuracy and computation complexity [12]. Regarding the SOC algorithm, many closed-loop observers, such as a Kalman filter (KF) and its advanced modifications, particle filter (PF) [13], and $H\infty$ filter [14], in addition to others [15, 16], are implemented to calculate the precise SOC value. Among these closed-loop observers, the KF algorithm and its advanced modifications, such as extended Kalman filter (EKF) [17-19], adaptive extended Kalman filter (AEKF) [20], unscented Kalman filter (UKF) [21], and strong tracking extended Kalman filter (STEKF) [22], are massively researched for their capability to solve random noise and for their low computational burden in a BMS. At present, for the research of model-based SOC estimation methods, many studies have comparatively studied the different ECMs from various perspectives. For example, Hu [23] compared 12 ECMs in terms of tracking accuracy, complexity, and robustness, and concluded that the first-order resistance-capacitor (RC) model is preferred for LiNMC batteries. He [24] compared 5 ECMs from the viewpoint of dynamic performance as well as SOC estimation accuracy, and concluded that the second-order RC model has the best dynamic performance and provides the most accurate SOC estimation. In addition, other researchers applied different system parameter identification methods for the same ECM and compared the quality of different identification methods [25, 26]. For the research of SOC estimation accuracy, numerous studies have compared the same ECM combined with different SOC estimation algorithms, such as EKF/UKF/PF, to obtain a result that the combination of which has the best estimation accuracy. For instance, Xia [27] compared two model-based adaptive algorithms, namely, the adaptive unscented Kalman filter (AUKF) and adaptive slide mode observer (ASMO), based on the second-order RC model, and concluded that these two approaches each have advantages. Yan [28] compared two KF algorithms, namely, the EKF and UKF, based on the first-order RC model, and concluded that the UKF algorithm is better than the EKF in both estimation accuracy and robustness.

However, in addition to the targets of the aforementioned research, there are still some problems worth studying. First, in view of the fact that the error sources of model-based SOC estimation algorithms mainly include model and measurement error, model error has a great influence on SOC estimation error. The specific relationship between model and SOC estimation error has been studied less, or nothing but qualitative descriptions given. To deeply understand the relationship between model and SOC estimation accuracy and improve the latter, it is necessary to qualitatively analyze the specific form between model and SOC estimation accuracy. Second, in engineering applications, choosing a suitable battery model is more reasonable than only pursuing the model accuracy, which means striking a balance between accuracy and complexity. Usually, the complexity of the battery model depends on what kinds of electronic components are used and the number of electronic components determines the computational burden for BMS chips in actual application. Thus, from this perspective, it is necessary to analyze the error sources of the model error and realize the influential level of each error source when the battery model is already determined. Once we know which error source has a greater impact, more attention can be paid to optimizing this part and the less influential part can be appropriately ignored. This strategy can not only maintain estimation accuracy but also reduce cost.

The main contributions of this paper are as follows: (1) to study the model and SOC estimation accuracy based on the first-order RC model and EKF algorithm under the constant current discharge (CCD) test and Federal Urban Dynamic Schedule (FUDS) test at different test temperatures (0°C, 10°C, 20°C, 30°C, 40°C, and 50°C); (2) to evaluate the specific relationship between the model and SOC estimation error by regression analysis and correlation analysis; and (3) to systematically study the impact of the SOC-OCV curve, Ohmic resistance, impedance, and sensor error on SOC estimation accuracy.

The rest of the article is organized as follows. In Section 2, the experimental setup is described. The battery model, parameter identification results, and EKF-based SOC observer are introduced in Section 3. Results are discussed in Section 4 and conclusions presented in Section 5.

2. EXPERIMENTAL SET-UP

2.1 Test Bench

The experimental test bench mainly consists of (1) 18650 cylindrical graphite/$LiNi_{1/3}Co_{1/3}Mn_{1/3}O_2$ batteries with a nominal capacity of 2.5 Ah and nominal voltage of 3.6 V; (2) a thermal temperature chamber with temperature control deviation less than 1°C; (3) a battery test system (Neware BTS-4002; voltage measurement range 0–5 V, current measurement range 0.1–30 A; the measurement deviation of current, voltage, and temperature sensors are within 0.2%); and (4) a host computer with Neware software installed for battery test control and data acquisition at 1-s intervals.

2.2 SOC-OCV Test

OCV is a critical parameter for both battery model and SOC estimation algorithms. It represents the terminal voltage of battery when it reaches the thermodynamic equilibrium state [29]. In this study, the OCV measurement steps are the following.

(1) The battery is fully charged by the constant current–constant voltage (CC-CV) method at the ambient temperature at which the battery is first charged under a constant current with a 1/3-C rate (approximately 0.833 A) until the voltage reaches 4.2 V, and then followed by a constant-voltage charge procedure until the current decreases to 1/25 C (approximately 0.1 A). Next, the SOC is regarded as 100%.

(2) Rest the battery inside the thermal chamber at the tested temperatures (0°C, 10°C, 20°C, 30°C, 40°C, and 50°C) for 2 h to reach the thermodynamic equilibrium state; the terminal voltage at that moment is considered as the OCV at 100% SOC.

(3) The battery is discharged under a constant current with a 1/25-C rate and the terminal voltage measured every 5% SOC interval. Finally, the terminal voltage reaches the cutoff voltage of 2.5 V and then the battery for is rested for 2 h.

(4) The battery is charged under a constant current with a 1/25-C rate and the terminal voltage measured every 5% SOC interval. Finally, when the terminal voltage reaches 4.2 V, the average value

of charge and discharge terminal voltage is regarded as the OCV since the effects of hysteresis and Ohmic resistance are reduced by the averaging [4].

2.3 Model Identification Test

For the identification of the model parameters, e.g., Ohmic resistance, polarization resistance, and polarization capacitance, the typical hybrid power pulse characterization (HPPC) test [30] is conducted at different tested temperatures (0°C, 10°C, 20°C, 30°C, 40°C, and 50°C). The test procedures are the following.

(1) The battery is fully charged by the CC-CV method at the ambient temperature and then rested inside the thermal chamber at the tested temperatures (0°C, 10°C, 20°C, 30°C, 40°C, and 50°C) for 2 h to reach the thermodynamic equilibrium state.

(2) As shown in Figure 1, the current profile of one hybrid power pulse sequence consists of a 30-s constant current discharge, and then a 40-s resting interval followed by a 10-s charge.

(3) The battery is discharged with a 1/3-C rate (approximately 0.833 A) to reach the 5% depth of discharge to the next SOC point and then rested for 1 h.

After that, the test steps (1)–(3) are repeated 20 times to cover the SOC range from 100% to 5%.

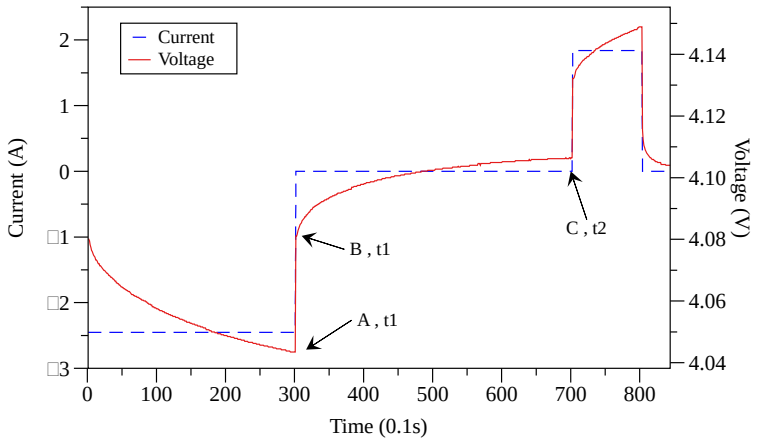

Figure 1. Current and voltage curves of one HPPC sequence

In addition, since the maximum available capacity of the battery is an essential parameter in the model-based SOC estimation algorithm and has a certain dependency on temperature, it is necessary to calibrate the maximum available capacity at various temperatures. In the work described in this article, the static capacity test was applied to measure the maximum available capacity; the test procedures are the following.

(1) The battery is fully charged by the CC-CV method at the ambient temperature and then rested inside the thermal chamber at the tested temperatures (0°C, 10°C, 20°C, 30°C, 40°C, and 50°C) for 2 h to reach the thermodynamic equilibrium state.

(2) The battery is discharged with a 1/3-C rate (approximately 0.833 A) until the terminal voltage reaches the cutoff voltage of 2.5 V and then rested for 2 h.

Test steps (1) and (2) are repeated three times and the average value is regarded as the maximum available capacity at a certain temperature

2.4 Validation Test

To fully validate the model and SOC estimation accuracy under relatively static and dynamic operating conditions, CCD and FUDS tests are conducted at various temperatures. For the CCD test, the battery is fully charged by the CC-CV method at the ambient temperature and then rested inside the thermal chamber at the tested temperatures (0°C, 10°C, 20°C, 30°C, 40°C, and 50°C) for 2 h. Then, the battery is discharged with a 1/3 C-rate (approximately 0.833 A) until the SOC reaches 10%. For the FUDS test, one typical sequence of FUDS cycle is 1372 s and, in this article, nine FUDS cycles are combined to build up the entire test to cover the wide range of SOCs. To implement the FUDS test on the sample battery, the battery size factor (BSF) was scaled down to 9.25 Wh. Likewise, the battery is fully charged by the CC-CD method and then rested at the tested temperature for 2 h before the FUDS test. The current profile of the entire FUDS test is shown in Figure 2. The positive current represents the discharging condition while the negative current the charging condition.

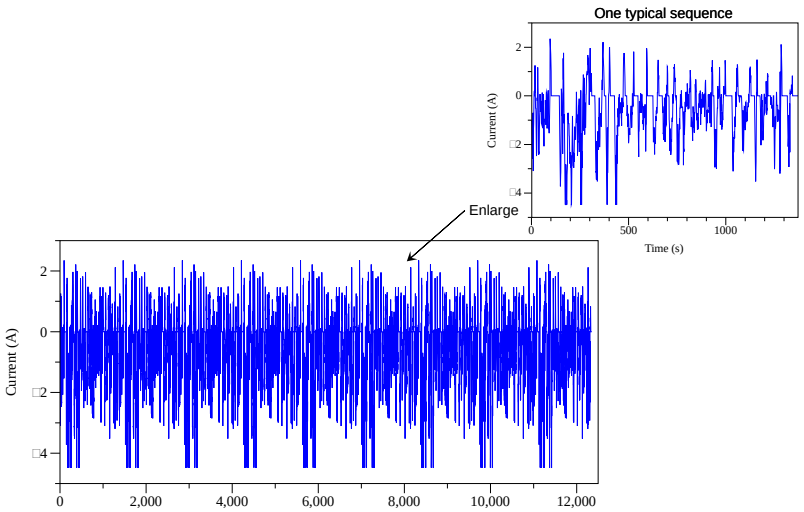

Figure 2. Current curve under FUDS test

3. MODEL-BASED SOC ESTIMATION ALGORITHM

3.1 Battery Model

Selecting an appropriate battery model is a primary and essential step for model-based SOC estimation approaches. Generally speaking, model accuracy and complexity are the main two factors that should be considered in practical application. On the one hand, model accuracy means that the selected model can reflect the characteristics of the battery precisely, especially highly non-linear and time-varying features. On the other hand, the model complexity indicates that the selected model has relatively low computational burden for BMS chips, so that it can be easily implemented in engineering applications. As discussed in the Introduction, it has been concluded in numerous studies that the first-

order RC model can maintain a great trade-off between model accuracy and complexity compared with other ECMs. In addition, the main targets of the present study are to analyze the correlation between model and SOC estimation accuracy and to determine the contribution of different parameters to the SOC estimation error. Therefore, the first-order RC model is chosen in this study and the model schematic is presented in Figure 3. The mathematical equations are

$$U_t = U_{oc} - U_p - R_0 I \quad , \qquad (1)$$

$$\overline{U_P} = -\frac{U_P}{C_P R_P} + \frac{I}{C_P} \quad , \qquad (2)$$

where U_{oc} represents the OCV, R_0 the Ohmic resistance, R_P the polarization resistance, C_P the polarization capacitance, U_t the terminal voltage measured by the voltage sensor, I the load current with a positive value for discharge and a negative value for charge, and U_p the voltage across the parallel RC network.

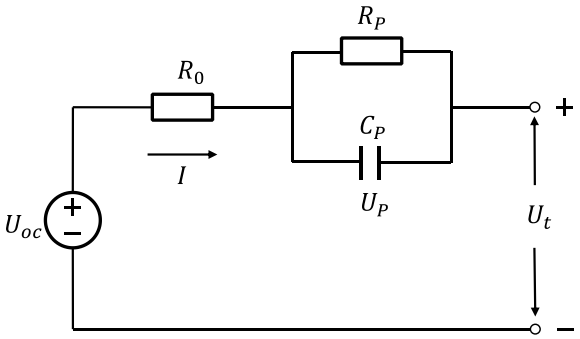

Figure 3. Schematic of the first-order RC model

3.2 Model Parameters Identification

According to the structure of the first-order RC model, the parameters that must be determined include OCV, R_0, R_P, C_P, and C_a, which, taken together, represent the maximum available capacity of battery.

3.2.1 SOC-OCV Identification

The SOC-OCV curves at different ambient temperatures are shown in Figure 4(a). It can be seen that the voltage difference mainly occurs in the high-SOC region (above 95% SOC) and low-SOC region (below 20% SOC), especially in the low-SOC region. Taking the voltage difference between 0°C and 50°C as an example, as shown in Figure 4(b), when the SOC decreases, the voltage difference continues to increase under 50% SOC, while the same phenomena can be found above 50% SOC. This is because as the temperature increases, the chemical reaction rate increases, and the activity of the positive electrode material is also enhanced. Thus, the battery can discharge much more electricity at high temperature and the Li^+ concentration in the electrodes is significantly different, which results in lower OCV. The same principle is suitable for the high-SOC region, so the battery can charge much more

electricity, resulting in the OCV at high temperature being higher than that at low temperature. For details of a similar phenomenon, Refs. [31-33] can be referred. As explained in Section 2.2, the effect of hysteresis is reduced by the averaging

Taking the fitting accuracy and computational complexity into consideration, the fourth-order polynomial is applied to fit the experiment data. The fitting functions of $U_{oc}(SOC)$ at different temperatures are summarized in Table 1 as are the evaluation indexes of fitting results.

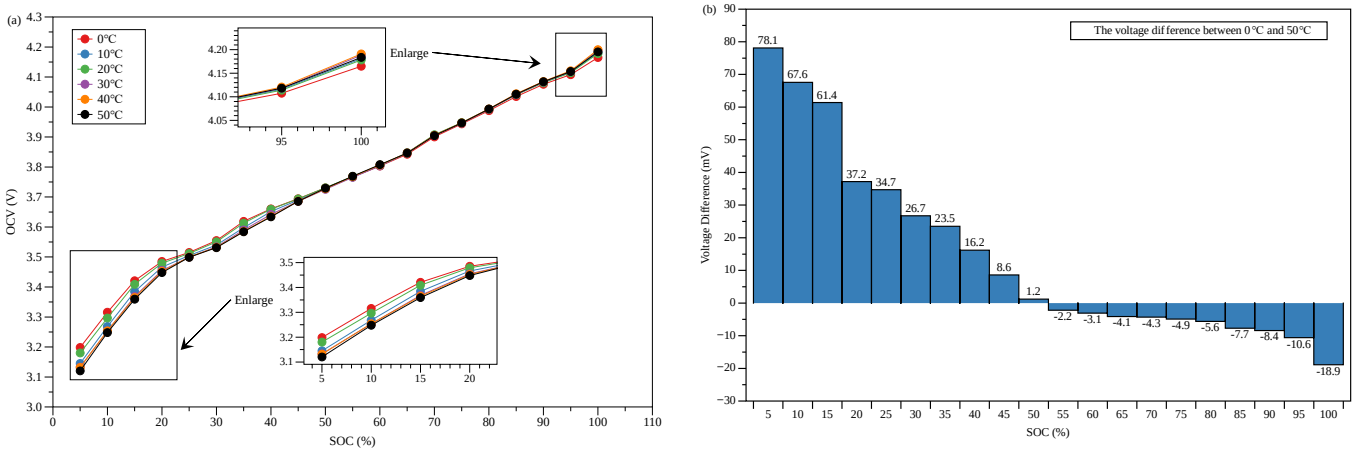

Figure 4. (a) SOC-OCV curves at different temperatures; (b) voltage difference between 0°C and 50°C

Table 1. Summary of polynomial fitting results

Temperature °C	Fitting Function	RMSE	R-square
0	$U_{oc} = -2.953 * SOC^4 + 7.288 * SOC^3 - 6.221 * SOC^2 + 2.965 * SOC + 3.074$	0.0108	0.9988
10	$U_{oc} = -3.061 * SOC^4 + 7.679 * SOC^3 - 6.744 * SOC^2 + 3.27 * SOC + 3.005$	0.0115	0.9988
20	$U_{oc} = -2.913 * SOC^4 + 7.279 * SOC^3 - 6.308 * SOC^2 + 3.056 * SOC + 3.05$	0.0114	0.9987
30	$U_{oc} = -2.836 * SOC^4 + 7.246 * SOC^3 - 6.464 * SOC^2 + 3.235 * SOC + 2.993$	0.0111	0.9989
4	$U_{oc} = -2.736 * SOC^4 + 7 * SOC^3 - 6.26 * SOC^2 + 3.177 * SOC + 2.995$	0.0114	0.9988
50°C	$U_{oc} = -2.88 * SOC^4 + 7.31 * SOC^3 - 6.515 * SOC^2 + 3.275 * SOC + 2.98$	0.0111	0.9989

3.2.2 R_0, R_P, C_P and C_a Identification

For the identification of R_0, R_P, C_P, and C_a, there are various methods to fit functions in the MATLAB (MathWorks, USA) simulation environment, such as the isqcurvefit command, polyfit command, and cftool box [34]. In this study, cftool was chosen to fit functions based on the data collected from the HPPC test since it provides a visual graphical interface and powerful curve-fitting ability. For

the specific procedures, Ref. [35] can be referred. Figure 5 shows the parameter identification results of R_0, R_P, C_P, and C_a at different temperatures.

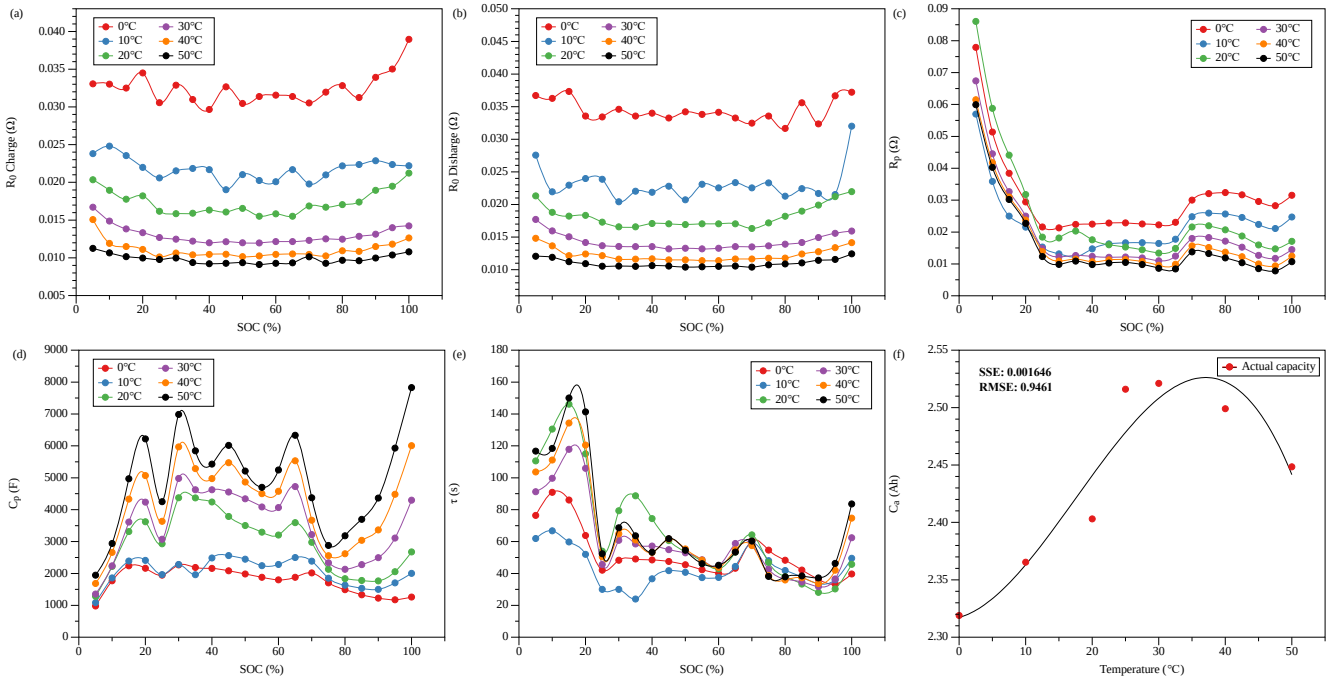

Figure 5. Parameter identification results of first-order RC model at different temperatures

As shown in Figure 5, it is clear to see that at low temperature (below 20°C) the parameters exhibit obvious differences between different temperatures, indicating that it is necessary to take the temperature variation into considerarion when identifying the parameters. One of the most obvious conditions is that the R_0 value increases significantly at 0°C, implying that the discharge performance of the battery would weaken. In addition, the R_0 value shows ruleless fluctuation at 0°C and 10°C as well. Regarding R_P and C_P, in addition to the temperature influence, these two parameters are extremely sensitive to SOC, which can be seen from the SOC range above 90% and below 20%. This phenomenon demonstrates that the battery has stronger non-linear features in the low-SOC range. According to Figure 5(f), C_a is calibrated at different temperatures and the fitting function is expressed as follows:

$$C_a = 2.321 + 0.0001376T_\infty + 0.0003996T_\infty^2 - 7.052e^{-6}T_\infty^3 \quad , \quad (3)$$

In actual simulation, except for the OCV and C_a, which use fitting equations to update real-time data, the remaining parameters are updated in real time using two-dimensional linear interpolation, which takes the temperature variation and SOC variation into consideration.

3.3 Model-based SOC Observer

Generally speaking, the EKF algorithm utilizes the input and output data to recursively optimize the system state adaptively. For the sake of simplicity, only the noteworthy points are introduced; more

detailed information can be found in the extensive literature within this field [17-19, 36]. The discretized state-space equations of a non-linear system can be described as follows:

$$x_{k+1} = f(x_k, u_k) + w_k \quad , \quad (4)$$

$$y_k = g(x_k, u_k) + v_k \quad , \quad (5)$$

Here, $x_k \in R^n$ is the state vector at time index k and Eq. (4) is called the "state equation" or "process equation." $u_k \in R^p$ is the known input to the system. $y_k \in R^m$ is the measured output and Eq. (5) is called the "measurement equation." w_k models the unmeasured input noise, which affects the state of the system, and v_k models the "sensor noise," which affects the measurement of the system. Both w_k and v_k are assumed to be mutually uncorrelated white Gaussian random processes with zero mean, and the covariance matrices can be defined as follows:

$$E[w_k w_k^T] = \begin{cases} Q_k, n = k \\ 0,\ n \neq k \end{cases} \quad , \quad (6)$$

$$E[v_k v_k^T] = \begin{cases} R_k, n = k \\ 0,\ n \neq k \end{cases} \quad , \quad (7)$$

where Q_k and R_k are pre-established values. $f(x_k, u_k)$ is a non-linear state transition function and $g(x_k, u_k)$ a non-linear measurement function that can be linearized by a first-order Taylor-series expansion at each time step as follows:

$$f(x_k, u_k) \approx f(\hat{x}_k, u_k) + \frac{\partial f(x_k, u_k)}{\partial x_k}|_{x_k = \hat{x}_k}(x_k - \hat{x}_k) \quad , \quad (8)$$

$$g(x_k, u_k) \approx g(\hat{x}_k, u_k) + \frac{\partial g(x_k, u_k)}{\partial x_k}|_{x_k = \hat{x}_k}(x_k - \hat{x}_k) \quad , \quad (9)$$

and $\hat{A}_k = \frac{\partial f(x_k, u_k)}{\partial x_k}|_{x_k = \hat{x}_k}$, $\hat{C}_k = \frac{\partial g(x_k, u_k)}{\partial x_k}|_{x_k = \hat{x}_k}$.

The battery model equations in Section 3.1 are transformed into discretized form, Eqs. (10) and (11). Then, combining Eqs. (12), the model-based EKF algorithm is built.

$$U_{t.k} = U_{oc.k}(SOC) - U_{P.k} - R_{0.k} I_k + v_k \quad , \quad (10)$$

$$U_{P.k} = U_{P.k-1} \exp\left(\frac{-\Delta t}{\tau_k}\right) + R_{P.k-1}\left(1 - \exp\left(\frac{-\Delta t}{\tau_k}\right)\right) I_{k-1} + w_{2.k-1} \quad , \quad (11)$$

$$SOC_k = SOC_{k-1} + \frac{\Delta t \cdot \eta \cdot I_k}{C_a \cdot 3600} + w_{1.k-1} \quad , \quad (12)$$

$$x_k = \begin{pmatrix} SOC_k \\ U_{P.k} \end{pmatrix} \quad , \quad (13)$$

$$\hat{A}_k = \frac{\partial f(x_k, u_k)}{\partial x_k}|_{x_k = \hat{x}_k^+} = \begin{pmatrix} 1 & 0 \\ 0 & \exp\left(\frac{-\Delta t}{\tau_k}\right) \end{pmatrix}|_{SOC = \widehat{SOC}_k^+} \quad , \quad (14)$$

$$B_k = \begin{pmatrix} \frac{\Delta t \cdot \eta \cdot}{C_n \cdot 3600} \\ R_{P.k-1}\left(1 - \exp\left(\frac{-\Delta t}{\tau_k}\right)\right) \end{pmatrix} \quad , \quad (15)$$

$$\hat{C}_k = \frac{\partial g(x_k, u_k)}{\partial x_k}|_{x_k = \hat{x}_k^-} = \begin{pmatrix} \frac{\partial U_{OCV}}{\partial SOC}|_{\hat{x}_k^-} & -1 \end{pmatrix} \quad , \quad (16)$$

where C_a is the maximum available capacity of the battery and η the Coulomb efficiency, which is usually set as 1 when charging and 0.98 when discharging. SOC_k and $U_{P.k}$ are regarded as the state vectors at time index k, terminal voltage $U_{t.k}$ is the measured system output at time index k, and I_k is the known system input. The matrices $\hat{A}_k$ and $\hat{C}_k$ are calculated at each sample point. The EKF process is summarized in Table 2. According to the initial state of the battery before the CCD and FUDS tests, the initial values of the EKF algorithm are set as $SOC_0 = 1$ and $U_{P.0} = 0$. Meanwhile, to ensure the reliability of the present study, the tuning values are all set as P_0^+=[0.089 0; 0 0.001], $R_k = [0.001]$, and $Q_k = [0.01\ 0; 0\ 0.0001]$, which can be considered the optimal settings.

Table 2. Summary of EKF algorithm process

Definitions:
$\hat{A}_k = \frac{\partial f(x_k,u_k)}{\partial x_k}\|_{x_k=\hat{x}_k^+}, \hat{C}_k = \frac{\partial g(x_k,u_k)}{\partial x_k}\|_{x_k=\hat{x}_k^-}$
Step 1: Initialization, For $k = 0$,
$\hat{x}_0^+ = E(x_0), P_0^+ = E[(x_0 - \hat{x}_0)(x_0 - \hat{x}_0)^T]$
Step 2: Computation, For $k = 1,2,3, ...,$ compute
Time update:
$\hat{x}_k^- = \hat{A}_{k-1}\hat{x}_{k-1}^- + B_{k-1}u_k$
$P_k^- = \hat{A}_{k-1}P_{k-1}^+\hat{A}_{k-1}^T + Q_k$
Kalman gain:
$L_k = P_k^-\hat{C}_k^T(\hat{C}_kP_k^-\hat{C}_k^T + R_k)^{-1}$
Measurement update:
$\hat{x}_k^+ = \hat{x}_k^- + L_k[y_k - g(\hat{x}_k^-, u_k)]$
$P_k^+ = (I - L_k\hat{C}_k)P_k^-$

4. RESULTS AND DISCUSSION

4.1 Analysis of model accuracy and SOC estimation accuracy

4.1.1 Analysis of battery model accuracy

Building an accurate and reliable battery model is of great importance for all model-based SOC estimation approaches. Therefore, it is first necessary to validate the model accuracy. The model accuracy is evaluated by the mean absolute error (MAE) of the terminal voltage error and root mean square error (RMSE) of the terminal voltage error. To compare the influence of different parameter identification results on model and SOC estimation accuracy, three estimators are built, namely, *F(SOC,T)*, *F(SOC,30°C)*, and *F(50%,30°C)*. The *F(SOC,T)* estimator represents that the parameters (e.g., SOC-OCV curve, R_0, R_P, and C_P) used in the first-order model are real-time, two-dimensional linear interpolations of SOC and temperature to consider the influence of SOC variation and temperature variation. The *F(SOC,30°C)* estimator represents that the parameters used in the first-order model are one-dimensional linear interpolations of SOC at 30°C to ignore the impact of temperature on parameters. The *F(50%,30°C)* estimator represents that the parameters used in the first-order model are fixed values identified at 50% SOC and 30°C. The specific results of all three models are summarized in Table 3. The comparison of *F(SOC,T)* between the experimental and simulated terminal voltages, as well as the voltage error under the CCD and FUDS tests at different temperatures, are shown in Figures 6 and 7, respectively. Figure 8 compares the statistical indices of the three models

According to the comparison between the experiment and simulated terminal voltages in Figures 6(a) and 7(a), it can be seen that the model exhibits great voltage tracking ability under both CCD and FUDS tests at different temperatures, manifesting that the model can simulate the dynamic characteristic of a battery well. Comparing the voltage error under both CCD and FUDS tests at different temperatures

in Figures 6(b) and 7(b), one can find that large errors and the error fluctuation mainly occur at the beginning and approaching the end of tests, in other words, during the high- and low-SOC regions. These phenomena are due to the highly non-linear characteristic in high- and low-SOC regions that lead to difficulties in voltage tracking, which can be seen from parameter identification results as well. In addition, from the perspective of temperature compensation, the model accuracy improves greatly when the parameter identification results take temperature variation into consideration, especially at 0°C and 10°C, as shown in the Figure 8. For example, comparing the RMSE of *F(SOC,T)* with that of *F(SOC,30°C)*, the model error decreases by 37.87% and 40.8%, respectively, under the CCD and FUDS tests at 0°C, while decreasing by 49.33% and 57.41%, respectively, at 10°C. However, in the temperature range 20°C–50°C, the temperature variation has little impact on model accuracy, and even the simulated results of *F(50%,30°C)* used fixed values of model parameters that are close to the others. This is because in the temperature range 20°C–50°C and wide range of SOCs, the values of identified parameters are relatively stable. This principle is rather valuable in engineering applications since two-dimensional linear interpolation would occupy more BMS memory than fixed values. In summary, through the above analysis it can be concluded that high model accuracy in the low-SOC region and low temperature (below 20°C) must be further optimized, and, while taking temperature variation into consideration, can significantly improve model accuracy. In addition, in the temperature range 20°C–50°C, using fixed model parameters can obtain simulation results with similar accuracy.

Table 3. Summary of model errors at different temperatures

Validation Test	Units: mV		Test temperatures					
			0℃	10℃	20℃	30℃	40℃	50℃
CCD test	*F(SOC,T)*	MAE	32.2843	14.5665	22.2760	22.8138	16.1730	6.9753
		RMSE	37.3995	15.5052	23.2434	23.6334	18.0801	10.4269
	F(SOC,30℃)	MAE	55.0589	28.6388	22.2297	22.8513	13.4370	7.2380
		RMSE	60.1974	30.5985	24.1941	23.6649	16.5486	9.9973
	F(50%,30℃)	MAE	58.1416	29.1547	24.6854	25.0138	15.6692	7.4830
		RMSE	62.3294	32.0548	26.2595	25.8503	18.6971	10.7920
FUDS test	*F(SOC,T)*	MAE	31.2798	10.9883	18.6276	26.5622	18.7592	8.0671
		RMSE	37.3798	13.1914	20.3606	29.5818	20.8899	10.3231
	F(SOC,30℃)	MAE	49.3587	24.7819	18.1714	26.5622	18.0771	7.5100
		RMSE	63.1445	30.9735	21.4037	29.5818	20.9409	10.0856
	F(50%,30℃)	MAE	51.3236	25.3087	19.7280	28.5796	20.1631	7.6807
		RMSE	66.4159	32.369	23.4212	32.2518	23.3287	10.2780

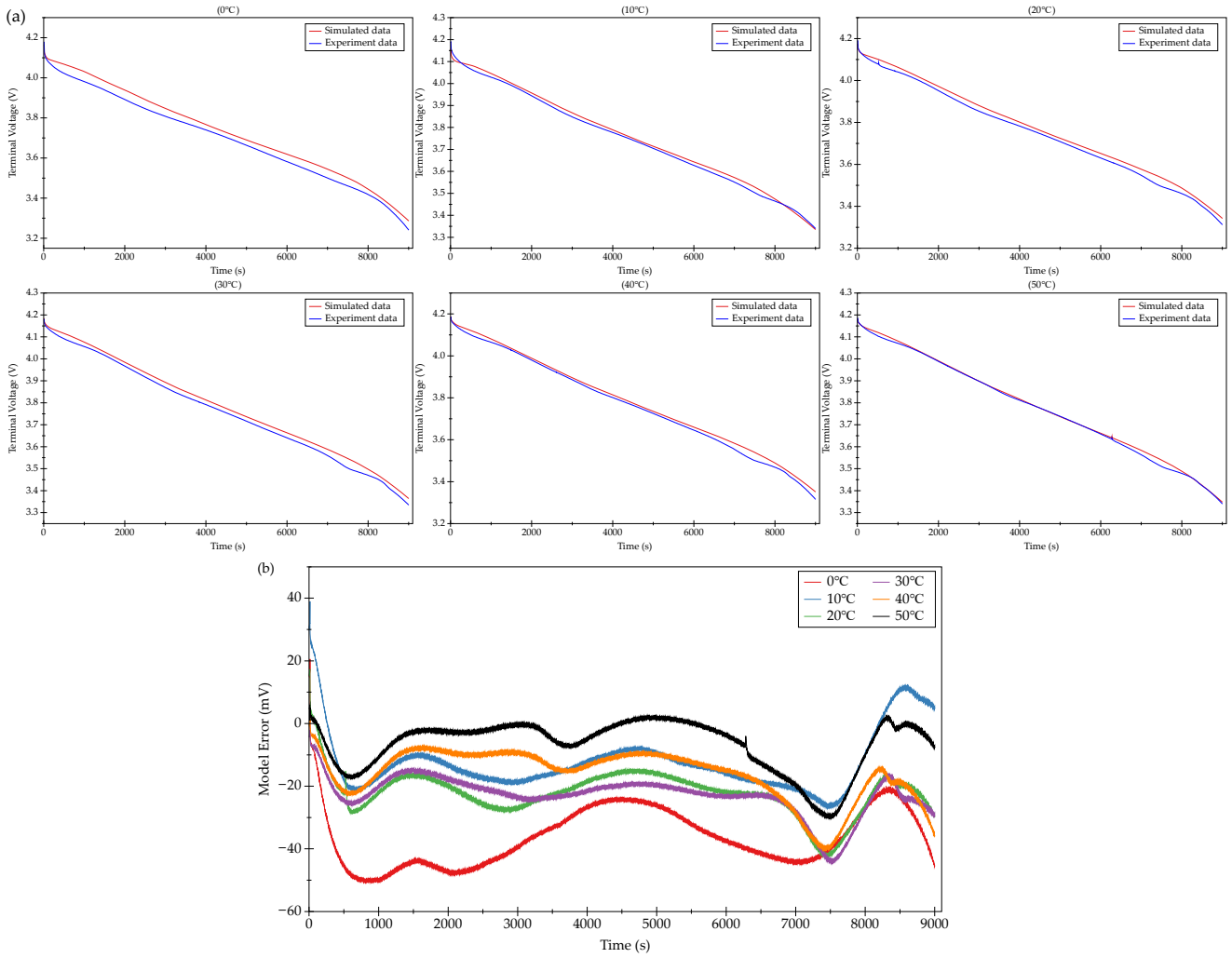

Figure 6. Results of model accuracy under CCD test at different temperatures: (a) Comparison between experimental and simulated terminal voltages; (b) model error

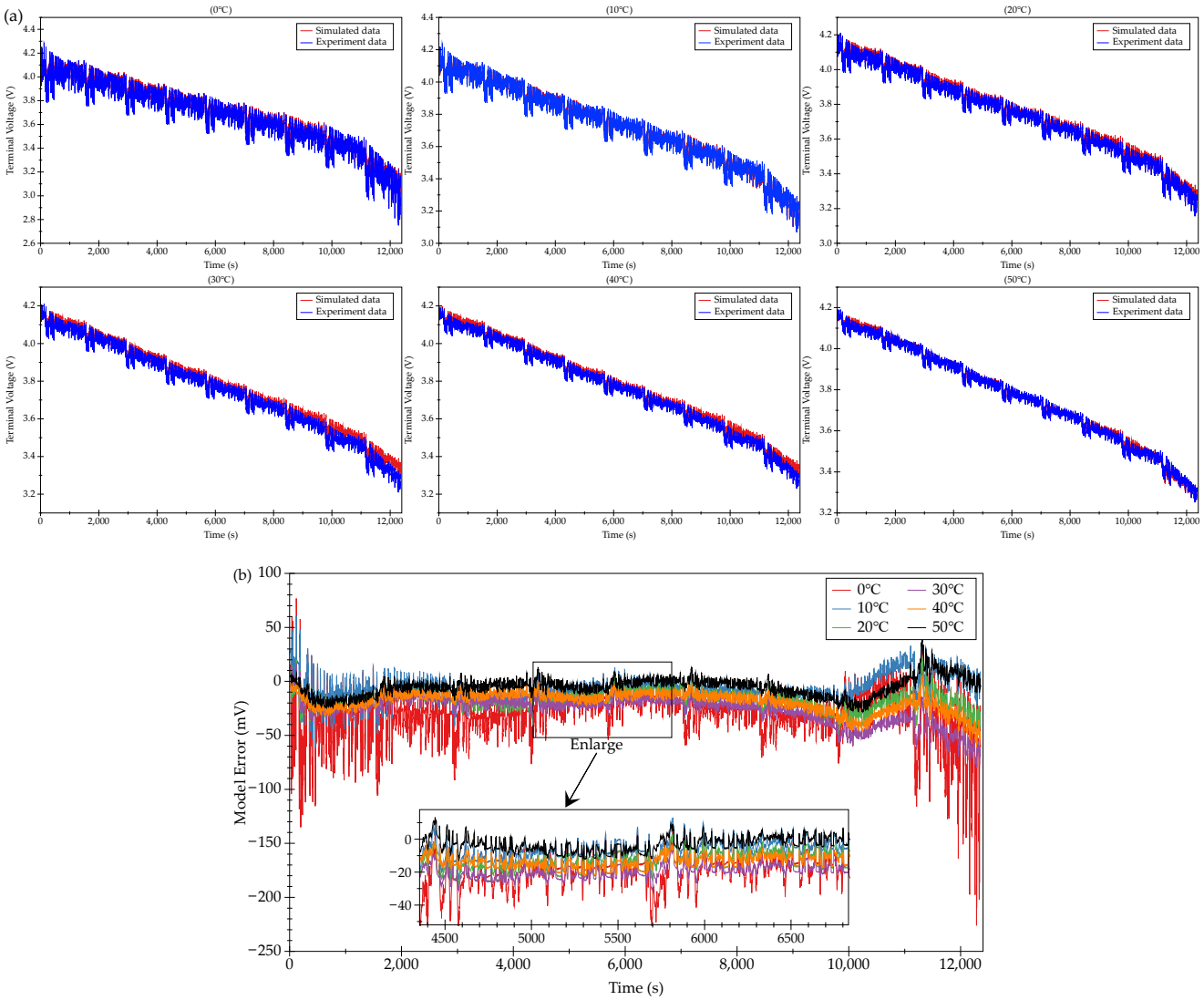

Figure 7. Results of model accuracy under FUDS test at different temperatures: (a) Comparison between experimental and simulated terminal voltages; (b) model error

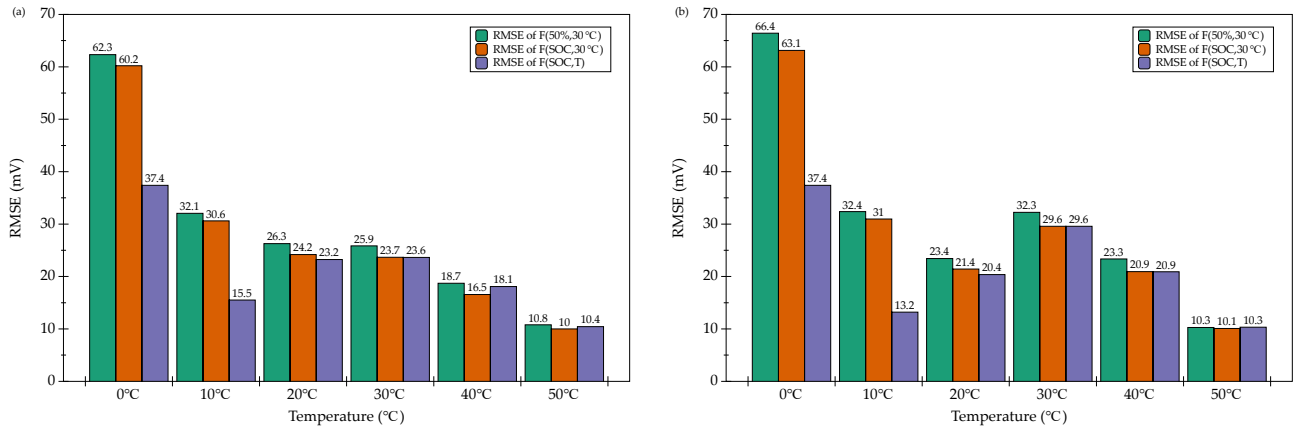

Figure 8. RMSEs of three models error at different temperatures: (a) CCD test; (b) FUDS test

4.1.2 Analysis of the SOC Estimation Accuracy

In this subsection, the accuracy of three SOC estimators based on the EKF algorithm are systematically analyzed under CCD and FUDS tests at different temperatures. Likewise, two statistical indices, namely, both the MAE and RMSE of the SOC estimation error, are applied to evaluate the SOC estimation accuracy. Before the analysis, it is worth highlighting that the reference SOC is obtained directly by the ampere-hour integral method, since the initial value error, battery capacity error, and current measurement error can be eliminated artificially. Moreover, numerous studies [20, 28, 31] have applied this approach to obtain reference SOCs.

The specific results of the three aforementioned estimators are summarized in Table 4. The comparison of *F(SOC,T)* between the reference and estimated SOCs, as well as the estimation error under CCD and FUDS tests at different temperatures, are shown in Figures 9 and 10, respectively. Figure 11 compares the statistic indices of three estimators. Overall, the maximum RMSE of the *F(SOC,T)* estimator is less than 4.5% under both CCD and FUDS tests, demonstrating that the EKF algorithm has a good filtering function. Specifically, on the basis of the estimation error under both CCD and FUDS tests at different temperatures in Figures 9(b) and 10(b), it can be seen that large errors and the error fluctuation mainly occur at the beginning and approaching the end of tests, which is similar to the model error. From the perspective of temperature, the largest MAE and RMSE occur at 0°C under both CCD and FUDS tests, while at 50°C,the values of MAE and RMSE are both minimal. Moreover, as shown in Figure 11, it can be seen that when taking temperature variation into consideration the accuracy of SOC estimation improves greatly at low temperature (0°C and 10°C), but there is little impact at other temperatures. For instance, the MAE and RMSE decrease by 52.84% and 53.53%, respectively, under the FUDS test at 10°C, while at 20°C the RMSE only decreases by 2.5%. Therefore, the high accuracy of SOC estimation in the low-SOC region and at low temperature must be further improved.

It is worth noting that there are many similarities and correlations between model and SOC estimation accuracy, which are discussed in the next subsection.

Table 4. Summary of SOC estimation errors at different temperatures

Validation test	Units: %		Test temperatures					
			0°C	10°C	20°C	30°C	40°C	50°C
CCD test	*F(SOC,T)*	MAE	4.0765	1.6162	2.4000	2.4081	1.6433	0.7264
		RMSE	4.2538	1.7371	2.5271	2.5010	1.8046	1.0654
	F(SOC,30°C)	MAE	5.9301	3.0678	2.4095	2.4081	1.3402	0.7425
		RMSE	6.5033	3.3055	2.6154	2.5010	1.6110	1.0048
	F(50%,30°C)	MAE	6.2062	3.1880	2.6449	2.6204	1.5702	0.7467
		RMSE	6.7078	3.4858	2.8165	2.6834	1.7855	1.0637
FUDS test	*F(SOC,T)*	MAE	3.1567	1.1225	1.9609	2.6081	2.0081	0.7801
		RMSE	3.4695	1.307	2.0865	2.7513	2.1312	1.0196
	F(SOC,30°C)	MAE	4.5959	2.3804	1.8675	2.6081	1.7811	0.6610
		RMSE	5.4754	2.8131	2.1411	2.7583	1.9664	0.9266
	F(50%,30°C)	MAE	4.7955	2.4687	2.0344	2.8248	2.0013	0.7083
		RMSE	5.6872	2.9511	2.3159	2.9668	2.1573	0.9781

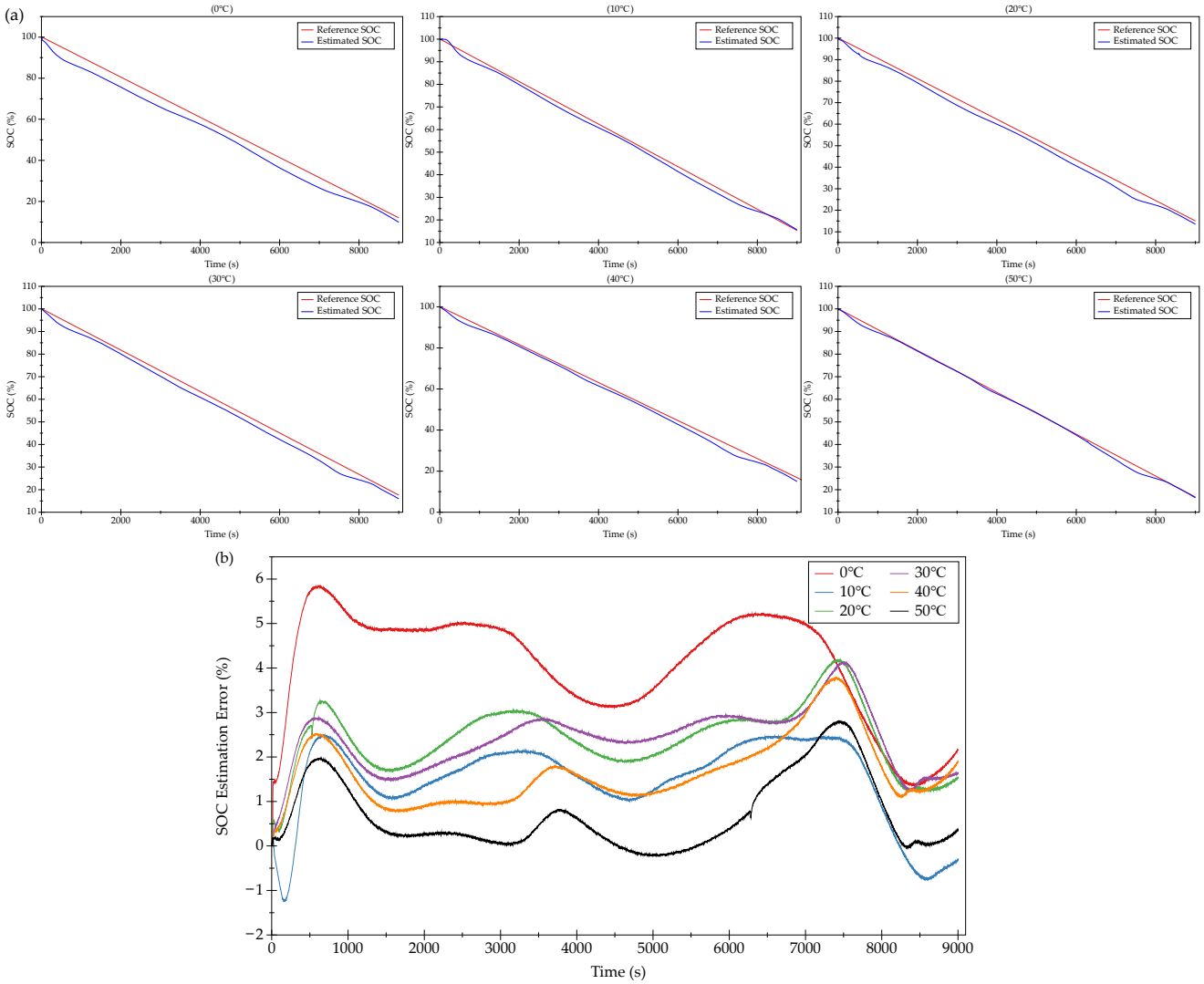

Figure 9. Results of SOC estimation accuracy under CCD test at different temperatures: (a) comparison between reference and estimated SOCs; (b) SOC estimation error

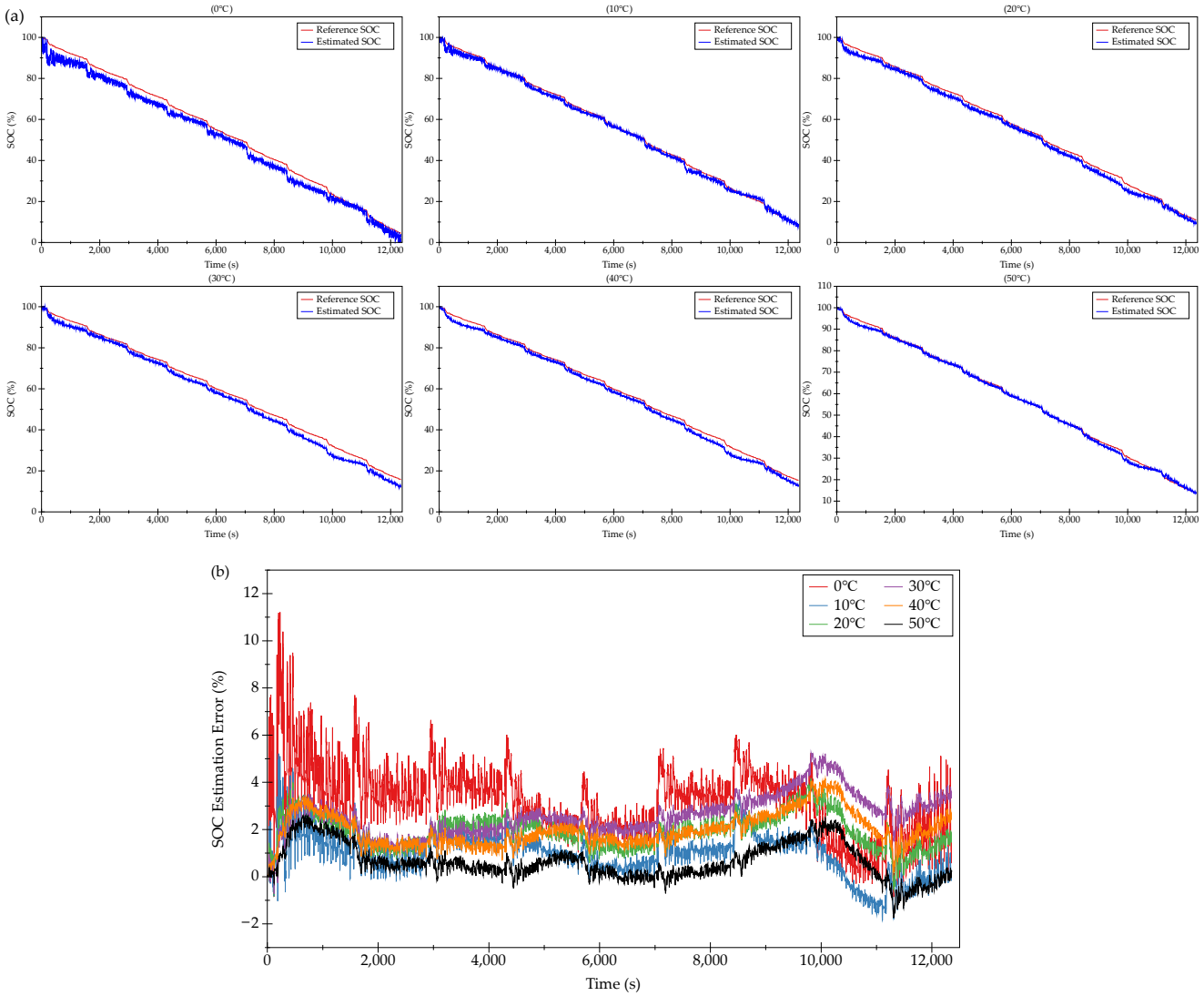

Figure 10. Results of SOC estimation accuracy under FUDS test at different temperatures: (a) comparison between reference and estimated SOCs; (b) SOC estimation error

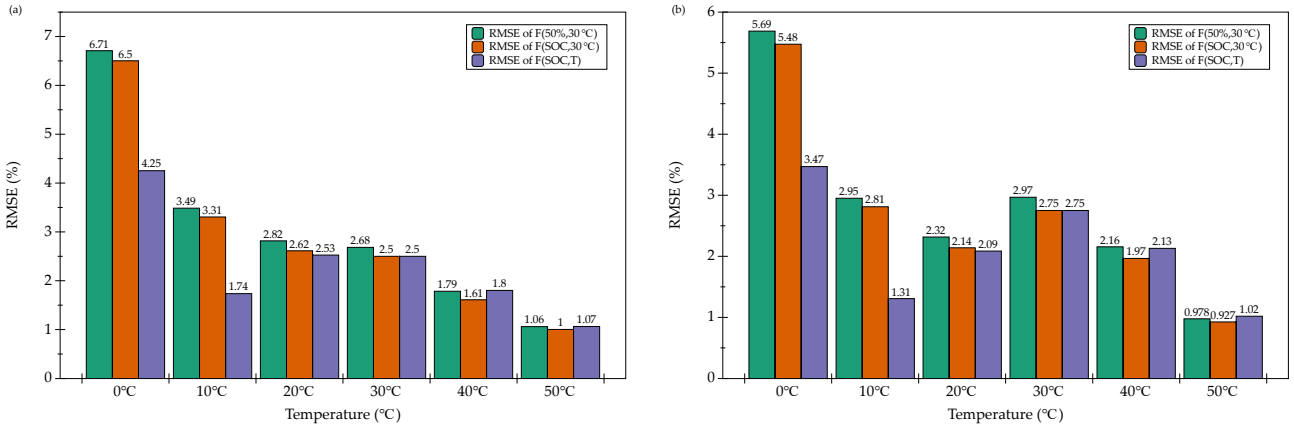

Figure 11. Comparison of RMSE of SOC estimation error at different temperatures: (a) CCD test; (b) FUDS test

4.1.3 Correlation Analysis between Model and SOC Estimation Accuracy

Through the analysis in the two preceding subsections, many similarities and the relationship between model and SOC estimation error can be found. For example, according to the comparison of model and SOC estimation error in Figure 12, one can always see that an increase in SOC estimation error is always accompanied by an increase in model error, and vice versa. This phenomenon clearly implies that there is a strong relationship between model and SOC estimation error. Moreover, according to the statistics of the RMSE of model and SOC estimation error in Tables 3 and 4, one can intuitively observe that when the model error is less than 20 mV, the corresponding SOC estimation error is usually less than 2%. This means that there is a monotonically increasing relationship between model and SOC estimation error. The main reason for these principles is that the essence of the EKF algorithm is the Gaussian fusion between the model and measured observations, and the fusion process is based on the battery terminal voltage when calculating SOC. However, the explanation above is a qualitative description and many studies reached a similar conclusion [12, 23, 24, 37]. As discussed in the Introduction, to deeply understand the relationship between model and SOC estimation accuracy, and improve SOC estimation accuracy, it is necessary to conduct a quantitative analysis and determine the specific relationship between model and SOC estimation error. In this article, regression and correlation analysis is conducted to study the specific relationship between model and SOC estimation error.

Since the RMSE is applied to evaluate the deviation between the real and estimated values, the regression and correlation analysis is introduced here to evaluate the relationship between the RMSE of model and SOC estimation error. First, the RMSE data in Tables 3 and 4 must be normalized because they have different units based on Eq. (17) (the new set of data are summarized in Table 5),

$$y' = \frac{y-min}{max-min} \quad , \quad (17)$$

where y is the original data, min and max are the minimum and maximum values of the original data, respectively, and y' is the normalized data.

Second, the Pearson correlation coefficient is usually used to assess the relationship between two sets of data in correlation analysis. When the absolute value of the Pearson correlation coefficient is closer to 1, it indicates that the two sets of data have stronger correlation. According to the results of correlation analysis shown in Table 6, the Pearson correlation coefficient is 0.981, close to 1, which manifests a high degree of linear positive correlation between the RMSE of both model and SOC estimation error. Then, on the basis of correlation analysis, regression analysis is conducted to determine the specific form between the two sets of data. Since there is a high degree of linear positive correlation between the RMSE of model and SOC estimation error, one-dimensional linear regression is determined by regression analysis and the specific form is shown as follows:

$$Y = A_0 + A_1 * X \quad , \quad (18)$$

Generally, the least-squares method is applied to calculate the two coefficients A_0 and A_1, which represent intercept and slope, respectively. The closeness of the regression line and the observation points is evaluated by R-square. The R-square value is closer to 1, which means that the regression equation can fit the data better. The R-square equation is expressed as follows:

$$R^2 = \frac{\sum(\hat{Y}-\bar{Y})^2}{\sum(Y-\bar{Y})^2} \quad , \quad (19)$$

According to Figure 13, all scatter points are evenly distributed on both sides of the fitting line. Moreover, according to the regression analysis results in Table 6, the R-square value is 0.96155, close to 1, demonstrating that the regression line with a slope of 0.9332 can follow the trend of the observation points well.

On the basis of the qualitative and quantitative analysis above, it can not only be concluded that the model accuracy has a great impact on SOC estimation accuracy, but it can be further concluded that there is a one-dimensional linear positive relationship between the model and SOC estimation error. One of the effective ways to improve SOC estimation accuracy is to improve the battery model accuracy. In the actual algorithm development process, we must first set the target of SOC estimation accuracy, and then choose the battery model, parameter identification method, and SOC estimation algorithm based on this target. Once the specific function between the model and SOC estimation accuracy is known, the battery model and parameter identification method with the least computational burden can be selected under the condition that the estimation accuracy can be guaranteed.

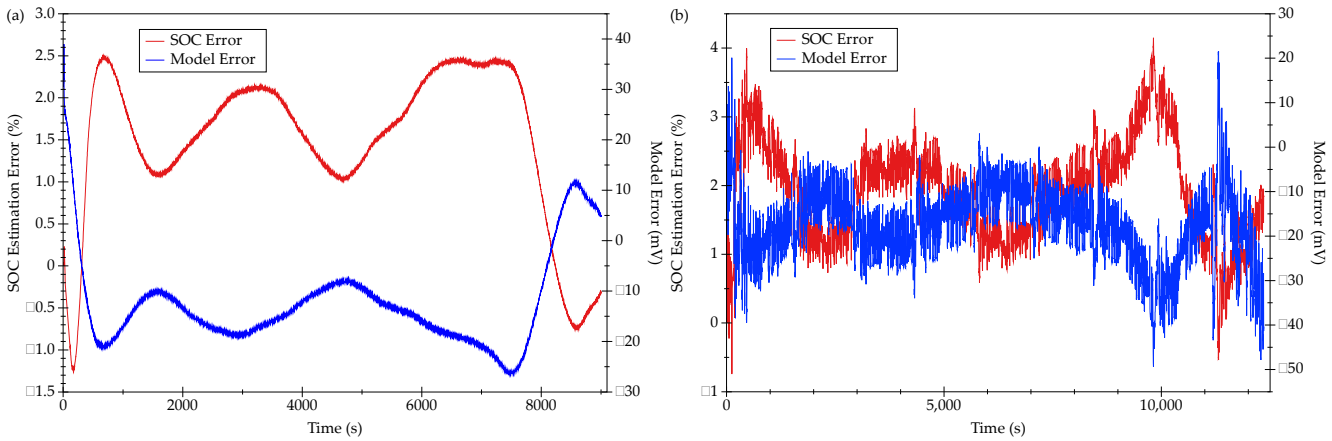

Figure 12. Comparison of model error and SOC estimation errors: (a) CCD test at 10°C; (b) FUDS test at 20°C

Table 5. Normalized RMSEs of model and SOC estimation errors

			0°C	10°C	20°C	30°C	40°C	50°C
Normalized RMSE of model error	CCD	*F(SOC,T)*	0.4856	0.0976	0.2347	0.2416	0.1432	0.0076
		F(SOC,30°C)	0.8897	0.3651	0.2516	0.2422	0.1161	0
		F(50%,30°C)	0.9275	0.3909	0.2882	0.2809	0.1542	0.0140
	FUDS	*F(SOC,T)*	0.4853	0.0566	0.1836	0.3471	0.1930	0.0057
		F(SOC,30°C)	0.9420	0.3717	0.2021	0.3471	0.1939	0.0015
		F(50%,30°C)	1	0.3965	0.2379	0.3944	0.2362	0.0049
Normalized RMSE of SOC estimation error	CCD	*F(SOC,T)*	0.5755	0.1401	0.2768	0.2723	0.1518	0.0240
		F(SOC,30°C)	0.9646	0.4114	0.2921	0.2723	0.1183	0.0135
		F(50%,30°C)	1	0.4426	0.3269	0.3038	0.1485	0.0237
	FUDS	*F(SOC,T)*	0.4398	0.0657	0.2006	0.3156	0.2083	0.0106
		F(SOC,30°C)	0.7868	0.3263	0.2100	0.3156	0.1798	0
		F(50%,30°C)	0.8234	0.3501	0.2403	0.3529	0.2128	0.0089

Table 6. Regression analysis and correlation analysis results of normalized RMSE

	Y=0.023024+0.9332*X
Residual sum of squares	2.68×10^{-5}
Pearson's r.	0.981
R-square	0.96155

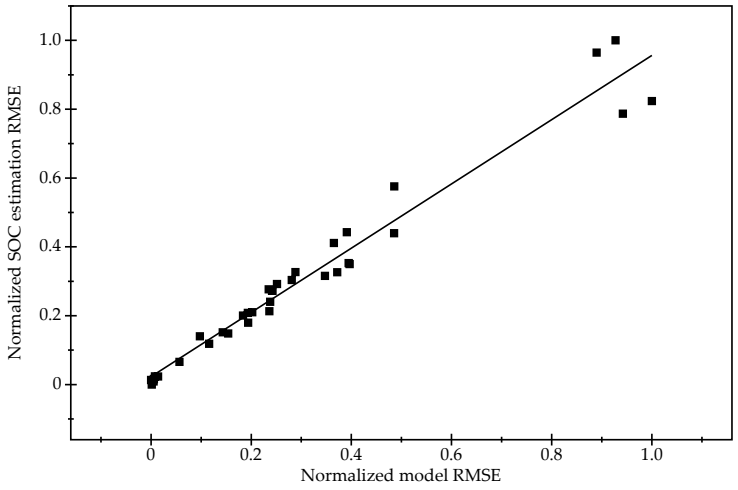

Figure 13. Scatter plot of relationship between normalized RMSE of model and SOC estimation error

4.2 Error Source Analysis of SOC Estimation Error

According to the analysis above, our conclusion is that there is a one-dimensional linear positive correlation between model and SOC estimation error. For model selection in practical applications, what is as important as accuracy and reliability is to take complexity regarding the model into account. Usually, the complexity of a battery model depends on what kinds of electronic components are used and the number of electronic components. Therefore, it is necessary to analyze the impact of different electronic components on SOC estimation error. In the following, the influence of model parameters, including Ohmic resistance, impedance, and SOC-OCV curve, on SOC estimation error is systematically analyzed. Moreover, in actual application, one of the fundamental function of a BMS is to monitor the state of a battery based on signals, e.g., voltage, current, and temperature, collected from different sensors. Therefore, the effect of sensor error on SOC estimation accuracy is worth studying as well. In the following subsections, therefore, the impact of voltage and current sensor measurement error on the accuracy of SOC estimation is also analyzed.

4.2.1 Impact of Model Parameters on SOC Estimation Accuracy

As discussed in Section 3.2.1, the SOC-OCV curve is sensitive to temperature, especially in the low-SOC region. The largest difference between 0°C and 50°C reaches 78 mV, as shown in Figure 4(b). In addition to the temperature, the SOC-OCV curve is also influenced by aging level [38]. Ohmic resistance in battery ECMs is usually considered an indicator with which to evaluate the discharge

performance or aging level of the battery. Thus, many researchers [39-41] applied different algorithms to identify Ohmic resistance in order to estimate SOP and SOH. The impedance in battery ECMs is used to simulate the non-linear polarization characteristics, including resistor, concentration, and activation polarization. As researched in Refs. [42, 43], the impedance growth increases significantly as the temperature and aging level increase. Therefore, all of the parameters can be considered as functions of temperature and aging level, and inaccurate parameter identification results would directly decrease the model and SOC estimation accuracy.

In this subsection, to compare the influence degree of different parameters on SOC estimation accuracy, it is assumed that the identified parameters are inaccurate, and the parameter errors are artificially added to the identification results in Section 3.2 using the single variable principle. Specifically, it is assumed that the SOC-OCV curve is inaccurate and the drift voltage varies from 0 mV, which means the SOC-OCV curve is accurate to 50 mV, which indicates that there is a great error in the SOC-OCV curve. For Ohmic resistance and impedance, it is assumed that the error gradually increases from 0% to 100%, where 0% represents the parameters are accurate and 100% represents that there is a great error. Meanwhile, three statistical indices are applied, namely, K_{ocv}, K_{R0}, and $K_{impedance}$, to separately evaluate the SOC estimation error caused by the inaccurate SOC-OCV curve, inaccurate Ohmic resistance, and inaccurate impedance at different temperatures, and the Equations are

$$K_{ocv} = \frac{RMSE_{drift}}{RMSE_{original}} \quad , \quad (20)$$

$$K_{R0} = \frac{RMSE_{Ro}}{RMSE_{original}} \quad , \quad (21)$$

$$K_{impedance} = \frac{RMSE_{impedance}}{RMSE_{original}} \quad , \quad (22)$$

where $RMSE_{original}$ represents the RMSE of SOC estimation with accurate parameters, $RMSE_{drift}$ the RMSE of SOC estimation with OCV drift, $RMSE_{R0}$ the RMSE of SOC estimation with inaccurate ohmic resistance, and $RMSE_{impedance}$ the RMSE of SOC estimation with inaccurate impedance.

The results under CCD and FUDS tests are shown in Figure 14. According to Figures 14(a) and (b), which depict the influence degree of an inaccurate SOC-OCV curve on SOC estimation accuracy, it can clearly be seen that the SOC estimation error increases by at least 2 times at all test temperatures. Specifically, the RMSE of SOC estimation is 1.0195% without drift voltage, and reaches 5.9013% with a drift voltage of 50 mV, which increases greatly, i.e., 6 times, under the FUDS test at 50°C. Likewise, under the CCD test, the RMSE of SOC estimation is 1.7371% without drift voltage and reaches 7.1337% with a drift voltage of 50 mV, which increases greatly, i.e., 4 times, at 10°C. Furthermore, it is interesting to note that the influence of an inaccurate SOC-OCV curve at 50°C under both CCD and FUDS tests is the greatest, while the influence is the least at 0°C, implying that higher accuracy of a SOC-OCV curve must be obtained at high temperature. According to Figures 14(c) and (d), which depict the influence level of inaccurate Ohmic resistance on SOC estimation accuracy, it can be seen that with the Ohmic resistance error increasing to 100%, the increments of SOC estimation error at all test temperature are less than 2 times, except at 10°C. For instance, under the FUDS test, the RMSE of SOC estimation is 2.501% without Ohmic resistance error and increases to 3.6913% with Ohmic resistance error increasing to 100%. Compared to the influence of an inaccurate SOC-OCV curve, the contribution of Ohmic resistance error to SOC estimation error is much less.

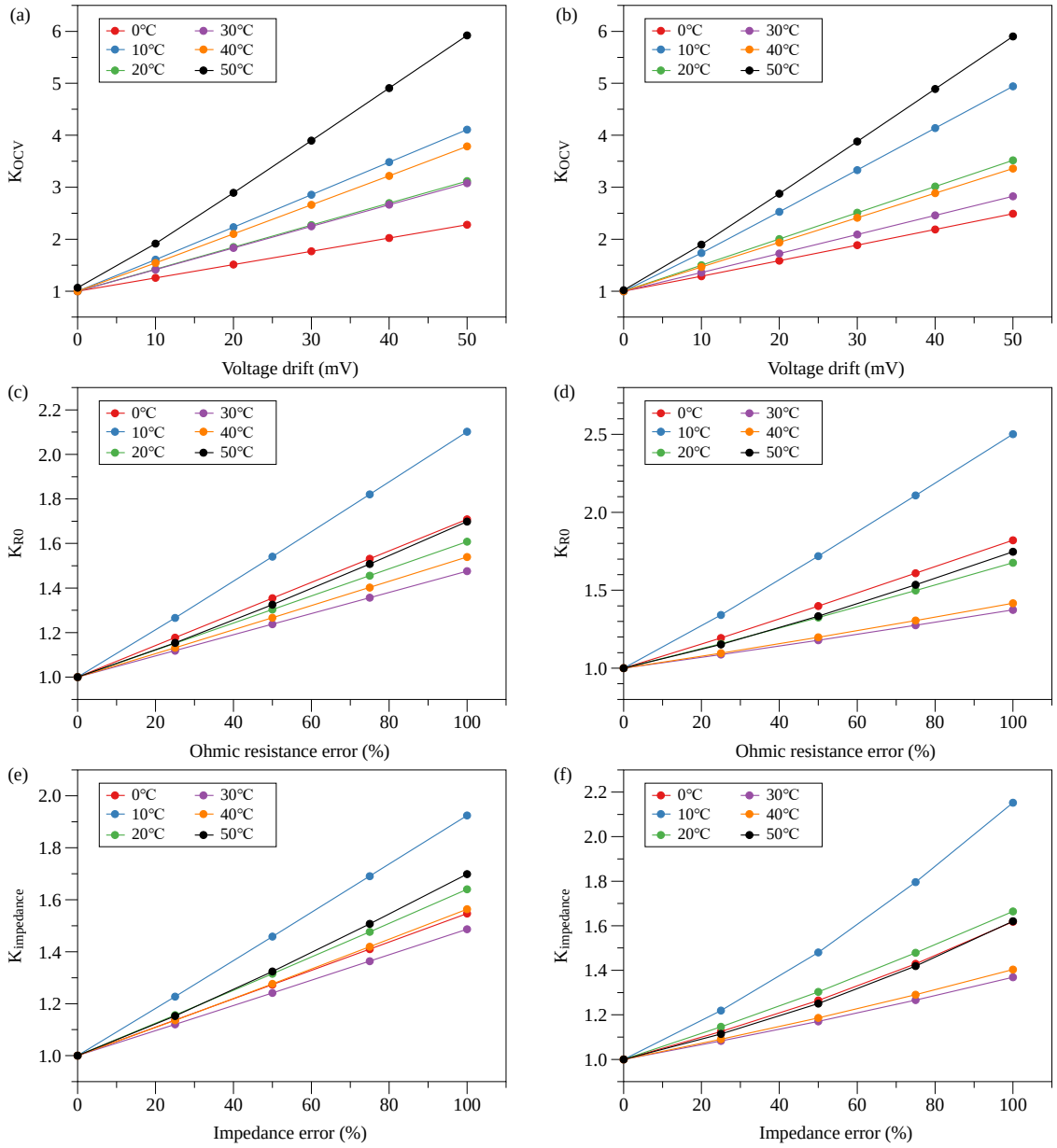

Figure 14. Impact of inaccurate parameters on SOC estimation at different temperatures: (a) inaccurate SOC-OCV curve under (a) CCD test and (b) FUDS test; inaccurate Ohmic resistance under (c) CCD test and (d) FUDS test; inaccurate impedance under (e) CCD test and (f) FUDS test

Regarding the impedance shown in Figures 14(e) and (f), with impedance error increasing to 100%, the increments of SOC estimation error at all test temperatures are less than 2 times, except at 10°C, which is similar to the Ohmic resistance error. Specifically, the RMSE of SOC estimation is 1.0195% without impedance error and increases to 1.6522% with impedance error increasing to 100% under the FUDS test at 50°C. Under the CCD test, the RMSE of SOC estimation is 1.0654% without equivalent impedance error and increases to 1.8101% with impedance error increasing to 100% test at 50°C. Therefore, it can be concluded that the influence level of impedance error is comparable to that of

Ohmic resistance error, which is much less compared with the SOC-OCV curve. From the perspective of temperature, the impact of inaccurate Ohmic resistance and inaccurate impedance on SOC estimation error is the largest at 10°C under both CCD and FUDS tests.

4.2.2 Impact of Sensor Error on SOC Estimation Accuracy

In actual BMS applications, sensor errors mainly include two categories: random error and system error. Since the EKF algorithm has a strong ability to solve random error, in this paper sensor system errors were the object of focus. Sensor system error can be regarded as an offset drift value added to the measured value [22]. For instance, the commonly used voltage acquisition chip in an actual BMS usually has a voltage error limitation of 10 mV and, for current sensor, this limitation is considered to be 0.1 A. To compare the impact of different sensor errors on SOC estimation accuracy, the fixed voltage and current errors are artificial added to the measurement value to obtain the SOC estimation error under CCD and FUDS tests at different temperatures. Figure 15 shows the comparison results. Overall, under both CCD and FUDS tests, the influence of voltage sensor error is much greater than that of a current sensor. For example, according to Figure 16(a), with a 10-mV drift voltage at 30°C, the RMSE of SOC estimation increases from 2.5% to 3.54%, for which the growth rate is 42.28%, while with a 0.1-A drift current the RMSE of SOC estimation increases to 2.73%, for which the growth rate is 12.14%. Moreover, under the FUDS test at 20°C, the RMSE increases from 2.09% to 3.12%, for which the growth rate is 49.76%, while with a 0.1-A drift current the RMSE increases to 2.38%, for which the growth rate is 14.29%. The same principle can be found under other operating conditions. Therefore, it can be concluded that sensor system errors have a significant impact on SOC estimation, and to improve SOC estimation accuracy, the precision of sensors must be further improved, especially that of voltage sensors.

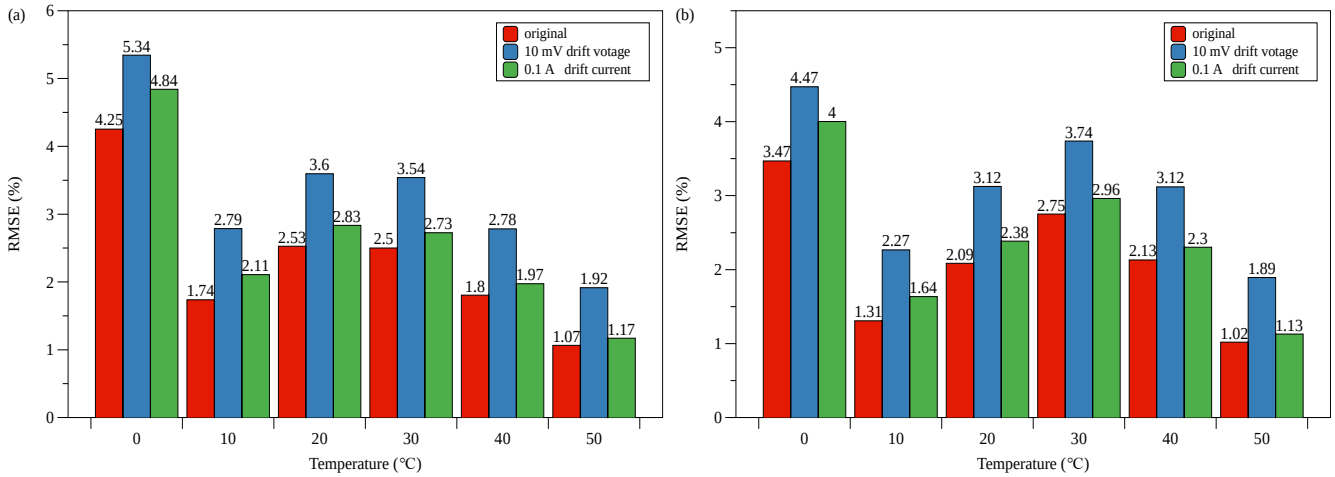

Figure 15. Impact of sensor errors on SOC estimation at different temperatures: (a) CCD test; (b) FUDS test

5. CONCLUSIONS

In this article, the model and SOC estimation accuracy based on the first-order RC model and EKF algorithm under CCD and FUDS tests at different test temperatures (0°C, 10°C, 20°C, 30°C, 40°C, and 50°C) is comprehensively studied. Second, regression and correlation analysis is applied to quantitatively evaluate the specific relationship between the RMSE of model and SOC estimation error. Third, the impact of the SOC-OCV curve, Ohmic resistance, impedance, and sensor error on SOC estimation accuracy is systematically studied. Based on the aforementioned results and analysis, the following conclusions are drawn.

(1) All of the parameters of the battery model are sensitive to temperature, especially low temperature (below 20°C). Thus, taking the temperature variation into consideration when identifying these parameters can significantly improve the model and SOC estimation accuracy. In addition, in the entire range of SOC, the largest model and SOC estimation errors mainly occur in the low-SOC region (below 20%), which manifests that high accuracy of the battery model and SOC estimation approach in the low-SOC region must be further optimized.

(2) On the basis of statistical analysis between the model and SOC estimation error, there are many similarities between model and SOC estimation error, and model accuracy has a strong impact on SOC estimation accuracy. The regression analysis and correlation analysis show that there is a one-dimensional linear positive relationship between the normalized RMSE of model and SOC estimation error.

(3) Among the parameters of the battery model, the accuracy of the SOC-OCV curve has the greatest influence on SOC estimation error compared to Ohmic resistance and impedance. In addition, the system sensor error has a great influence on SOC estimation. Compared to the effect of current sensor error, voltage sensor error has a more significant impact on SOC estimation.

On the basis of the conclusion of this article that there is a one-dimensional linear positive correlation between model and SOC estimation error, in planned future work, our focus will be on studying the relationship between different parameter identification approaches and different ECMs to determine a more accurate battery model with reasonable parameter identification results.

ACKNOWLEDGEMENTS

This work was supported by the National Natural Science Foundation of China (Grant No. 51775393); Hubei Province Technology Innovation Major Project (Grant No. 2018AAA054); the Fundamental Research Funds for the Central Universities (Grant No. 205207015); and the Innovation Research Team Development Program of the Ministry of Education of China (IRT_17R83).

References

1. M. A. Hannan, M. S. H. Lipu, A. Hussain and A. Mohamed, *Renewable Sustainable Energy Rev.*, 78 (2017) 834.
2. X. Hu, F. Feng, K. Liu, L. Zhang, J. Xie and B. Liu, *Renewable Sustainable Energy Rev.*, 114 (2019) 109334.

3. B. Jiang, H. Dai, X. Wei and T. Xu, *Appl. Energy*, 253 (2019) 113619.
4. F. Zheng, Y. Xing, J. Jiang, B. Sun, J. Kim and M. Pecht, *Appl. Energy*, 183 (2016) 513.
5. K. S. Ng, C.-S. Moo, Y.-P. Chen and Y.-C. Hsieh, *Appl. Energy*, 86 (2009) 1506.
6. F. Feng, S. L. Teng, K. L. Liu, J. L. Xie, Y. Xie, B. Liu and K. X. Li, *J. Power Sources*, 455 (2020) 14.
7. K. C. Wei, J. Wu, W. B. Ma and H. C. Li, *J. Eng.*, 2019 (2019) 9133.
8. Y. Shen, *Energy*, 152 (2018) 576.
9. P. Singh, R. Vinjamuri, X. Wang and D. Reisner, *J. Power Sources*, 162 (2006) 829.
10. Y. Zheng, M. Ouyang, X. Han, L. Lu and J. Li, *J. Power Sources*, 377 (2018) 161.
11. R. Xiong, L. Li, Q. Yu, Q. Jin and R. Yang, *J. Cleaner Prod.*, 249 (2020) 119380.
12. X. Lai, Y. Zheng and T. Sun, *Electrochim. Acta*, 259 (2018) 566.
13. Z. Chen, H. Sun, G. Dong, J. Wei and J. Wu, *J. Power Sources*, 414 (2019) 158.
14. L. Zhao, Z. Liu and G. Ji, *Control Eng. Pract.*, 81 (2018) 114.
15. B. Ning, B. Cao, B. Wang and Z. Zou, *Energy*, 153 (2018) 732.
16. J. Du, Z. Liu, Y. Wang and C. Wen, *Control Eng. Pract.*, 54 (2016) 81.
17. G. L. Plett, *J. Power Sources*, 134 (2004) 252.
18. G. L. Plett, *J. Power Sources*, 134 (2004) 277.
19. G. L. Plett, *J. Power Sources*, 134 (2004) 262.
20. J. P. Wang, J. G. Guo and L. Ding, *Energy Convers. Manag.*, 50 (2009) 3182.
21. G. Liu, C. Xu, K. Jiang and K. Wang, *Energy Procedia*, 158 (2019) 4477.
22. C. Zhang, F. W. Yan, C. Q. Du and G. Rizzoni, *Appl. Sci.-Basel*, 8 (2018) 27.
23. X. Hu, S. Li and H. Peng, *J. Power Sources*, 198 (2012) 359.
24. H. W. He, R. Xiong and J. X. Fan, *Energies*, 4 (2011) 582.
25. X. Lai, W. Gao, Y. Zheng, M. Ouyang, J. Li, X. Han and L. Zhou, *Electrochim. Acta*, 295 (2019) 1057.
26. H. Chun, J. Kim and S. Han, *IFAC-PapersOnLine*, 52 (2019) 129.
27. B. Xia, Z. Sun, R. Zhang, D. Cui, Z. Lao, W. Wang, W. Sun, Y. Lai and M. Wang, *Energies*, 10 (2017).
28. F. Yan, C. Zhang, C. Du and C. Cheng, *Int. J. Electrochem. Sci.*, 13 (2018) 12360.
29. Z. Li, J. Huang, B. Y. Liaw and J. Zhang, *J. Power Sources*, 348 (2017) 281.
30. T. Duong, *J. Power Sources*, 89 (2000) 244.
31. S. C. Yang, C. Deng, Y. L. Zhang and Y. L. He, *Energies*, 10 (2017) 14.
32. C. Campestrini, M. F. Horsche, I. Zilberman, T. Heil, T. Zimmermann and A. Jossen, *J. Storage Mater.*, 7 (2016) 38.
33. L. Lavigne, J. Sabatier, J. M. Francisco, F. Guillemard and A. Noury, *J. Power Sources*, 324 (2016) 694.
34. S. Nejad, D. T. Gladwin and D. A. Stone, *J. Power Sources*, 316 (2016) 183.
35. L. He, M. K. Hu, Y. J. Wei, B. J. Liu and Q. Shi, *Sci. China-Technol. Sci.*, 63 (2020) 410.
36. H. S. Ramadan, M. Becherif and F. Claude, *Int. J. Hydrogen Energy*, 42 (2017) 29033.
37. P. Shen, M. G. Ouyang, X. B. Han, X. N. Feng, L. G. Lu and J. Q. Li, *IEEE Trans. Veh. Technol.*, 67 (2018) 8055.
38. X. Bian, L. Liu, J. Yan, Z. Zou and R. Zhao, *J. Power Sources*, 448 (2020) 227401.
39. A. Farmann and D. U. Sauer, *J. Power Sources*, 329 (2016) 123.
40. P. Shen, M. G. Ouyang, L. G. Lu, J. Q. Li and X. N. Feng, *IEEE Trans. Veh. Technol.*, 67 (2018) 92.
41. N. Wassiliadis, J. Adermann, A. Frericks, M. Pak, C. Reiter, B. Lohmann and M. Lienkamp, *J. Storage Mater.*, 19 (2018) 73.
42. M. Ecker, N. Nieto, S. Käbitz, J. Schmalstieg, H. Blanke, A. Warnecke and D. U. Sauer, *J. Power Sources*, 248 (2014) 839.

43. K. Jalkanen, J. Karppinen, L. Skogström, T. Laurila, M. Nisula and K. Vuorilehto, *Appl. Energy*, 154 (2015) 160